



AIAA 2001-2616

**An Implicit Monolithic Time Accurate Finite
Element Scheme for Incompressible Flow
Problems**

Orlando Soto, Rainald Löhner and Juan Cebra
George Mason University
Fairfax, VA

**15th AIAA Computational Fluid Dynamics
Conference**

**11-14 June 2001
Anaheim, California**

An Implicit Monolithic Time Accurate Finite Element Scheme for Incompressible Flow Problems

O. Soto, R. Löhner and J. Cebal

SCS/Laboratory for Computational Fluid Dynamics - George Mason University, MS 4C7
4400 University Drive - Fairfax, VA 22030-4444, USA

e-mail: soto@scs.gmu.edu - web page: <http://www.science.gmu.edu/~lohner/>

Abstract

The objective of this paper is to develop an implicit, monolithic, finite element (FE) scheme for the solution of the incompressible Navier-Stokes (NS) equations. The design of the method is based on the pressure stability properties of an implicit second order in time fractional step (FS) method, which is conditionally stable. The final monolithic scheme preserves the second order accuracy of the FS method, and it is unconditionally stable (i.e. stable for all timestep sizes). In addition, it is shown that the final pressure stabilizing term is practically the same fourth order pressure term added by some authors, but following different arguments, to obtain high order accurate results. It is also shown that the final stabilized convective term is a formally second order discretization of the advective operator. Finally, a non-linear numerical switch was designed to lower the discretization order in flow regions where the solution could present over or undershoots, which can inhibit the algorithm convergence. Some numerical examples are presented.

1 Introduction

Among the schemes developed over the last decade for the solution of the incompressible NS equations (monolithic schemes [16, 13], projection or fractional step (FS) schemes [8, 19, 3, 22, 25, 20, 21], artificial compressibility (AC) [7, 26, 24, 23, 14, 18], preconditioning of the compressible NS equations [27, 6, 28], etc.) the FS schemes yields highly accurate pressure-stable results by integrating in an explicit manner the advective terms of the NS

equations. However, the timestep imposed by the smallest elements may be orders of magnitude smaller than the timestep required to obtain time-accurate results (physical timestep). For many classes of problems, e.g. biological flows (blood and air flow) and environmental flows (contaminant release), this implies tens of thousands of timesteps per simulation, rendering the schemes impractical. Most of the artificial compressibility and preconditioned schemes suffer from the same shortcoming.

On the other hand, the monolithic schemes treat, in general, the advective term in an implicit manner, which avoids the mentioned disadvantages. Nevertheless, these methods are very expensive from a computational point of view: the velocity and pressure discrete equations are coupled. For this reason, it is desirable to develop an implicit monolithic but uncoupled scheme, which is unconditionally stable, in order to allow using timestep sizes of the order of magnitude required for the physical problem.

To reach the mentioned objective, an implicit second order FS method is presented. The pressure stability of such approach holds only for timestep sizes larger than a critical one. This property is used to develop a stabilized monolithic scheme, which preserves the second order accuracy. The stabilized monolithic scheme is fractioned again to obtain an uncoupled algorithm for its solution. Finally, the splitting error of the last fractioned method is eliminated, obtaining the desired implicit second-order monolithic formulation, which is solved in an uncoupled manner. Some numerical examples are presented to verify the stability properties of the final method.

2 Second Order FE-FS scheme

The incompressible NS equations to be solved here are:

$$\frac{\partial \mathbf{u}}{\partial t} + (\mathbf{u} \cdot \nabla) \mathbf{u} - \nu \Delta \mathbf{u} + \nabla p = \mathbf{f} \quad \text{in } \Omega \times (0, t_f), \quad (1)$$

Copyright © 2001 by the authors. Published by the American Institute of Aeronautics and Astronautics, Inc. with permission.

$$\nabla \cdot \mathbf{u} = 0 \quad \text{in } \Omega \times (0, t_f) \quad (2)$$

where Ω is the flow domain, t is the time variable, $(0, t_f)$ the time interval for the simulation, \mathbf{u} the velocity field, ∇ the gradient operator, ν the kinematic viscosity, Δ the Laplacian operator, p the pressure and \mathbf{f} the external body forces (i.e. the gravity and the Boussinesq forces).

Let $\boldsymbol{\sigma}$ be the viscous stress tensor and \mathbf{n} the unit outward normal to the boundary $\partial\Omega$. Denoting by an overbar prescribed values, the boundary conditions for (2) to be considered here are:

$$\begin{aligned} \mathbf{u} &= \bar{\mathbf{u}} \quad \text{on } \Gamma_{\text{du}}, \quad p = \bar{p} \quad \text{and} \quad \mathbf{n} \cdot \boldsymbol{\sigma} = \bar{\mathbf{t}} \quad \text{on } \Gamma_{\text{nu}}, \\ \mathbf{u} \cdot \mathbf{n} &= \bar{u}_n, \quad \mathbf{n} \cdot \boldsymbol{\sigma} \cdot \mathbf{g}_1 = \bar{t}_1 \quad \text{and} \\ \mathbf{n} \cdot \boldsymbol{\sigma} \cdot \mathbf{g}_2 &= \bar{t}_2 \quad \text{on } \Gamma_{\text{mu}} \end{aligned} \quad (3)$$

for $t \in (t_0, t_f)$. The boundary $\partial\Omega$ has been considered split into three sets of disjoint components Γ_{du} , Γ_{nu} and Γ_{mu} , the latter being the part where mixed conditions are prescribed: the normal velocity and the tangent stresses. Vectors \mathbf{g}_1 and \mathbf{g}_2 (for the three-dimensional case) span the space tangent to Γ_{mu} . Finally, Γ_{du} and Γ_{nu} are the two disjoint components of $\partial\Omega$ where Dirichlet and Neumann boundary conditions for the velocity are prescribed. Initial conditions have to be appended to problem (2)-(3).

A classical implicit FS scheme for (2)-(3) is obtained by splitting the momentum equation in the standard manner, and by discretizing the temporal terms using the trapezoidal rule (or θ method). The resulting continuous problem, omitting the boundary and initial conditions for brevity, is as follows:

$$\frac{\delta \tilde{\mathbf{u}}}{\delta t} + \tilde{\mathbf{u}}^{n+\theta} \cdot \nabla \tilde{\mathbf{u}}^{n+\theta} + \nabla p^n - \nu \Delta \tilde{\mathbf{u}}^{n+\theta} = \mathbf{f}^{n+\theta} \quad (4)$$

$$\delta t \nabla^2 (p^{n+1} - p^n) = \nabla \cdot \tilde{\mathbf{u}}^{n+1}, \quad (5)$$

$$\frac{u^{n+1} - \tilde{u}^{n+1}}{\delta t} + \nabla (p^{n+1} - p^n) = 0 \quad (6)$$

where $\delta \tilde{\mathbf{u}} = \tilde{\mathbf{u}}^{n+1} - \mathbf{u}^n$, the superscripts n and θ refer to the time step and to the trapezoidal rule discretization parameter, respectively. $\tilde{\mathbf{u}}$ is the intermediate velocity, which is introduced to allow the momentum splitting. For $\theta = 1$ the standard backward Euler scheme is obtained, which has a temporal error of $O(\delta t)$. The value $\theta = 0.5$ gives the standard Crank Nicholson scheme, which is second order accurate in time $O(\delta t^2)$.

The error due to taking implicit advective and viscous terms in (4) can be estimated in a straightforward manner by obtaining $\tilde{\mathbf{u}}^{n+1}$ from (6), taking into account that $\tilde{\mathbf{u}}^{n+\theta} = \theta \tilde{\mathbf{u}}^{n+1} + (1 - \theta) \tilde{\mathbf{u}}^n$, and introducing the result in (4). The final expression is:

$$\frac{\mathbf{u}^{n+1} - \mathbf{u}^n}{\delta t} + \mathbf{u}^{n+\theta} \cdot \nabla \mathbf{u}^{n+\theta} + \nabla p^{n+1} - \nu \Delta \mathbf{u}^{n+\theta}$$

$$\begin{aligned} &= \mathbf{f}^{n+\theta} - \delta t \nabla \delta p^{n+\theta} \cdot \nabla (\mathbf{u}^{n+\theta} + \delta t \nabla \delta p^{n+\theta}) \\ &\quad + \delta t \nabla \cdot \left(2\nu \nabla (\nabla \delta p^{n+\theta}) \right) \end{aligned} \quad (7)$$

where $\delta p^{n+\theta} = \theta(p^{n+1} - p^n) + (1 - \theta)(p^n - p^{n-1})$.

Clearly the first five terms of (7) are the momentum equation discretized in time using the θ method, and the final two the error, which are of order $O(\delta t^\gamma)$ with $\gamma \geq 2$. Hence, the error of the implicit scheme is of the same order than the error of the stabilizing term $O(\delta t^2)$ (first term of (5)), and therefore, it has the same order of approximation than an explicit FS scheme.

The variational discrete form of (4)-(6) is: Given (\mathbf{u}_h^n, p_h^n) , find $(\mathbf{u}_h^{n+1}, p_h^{n+1})$ in $\mathbf{V}_h \times Q_h$ such that

$$\begin{aligned} &\frac{1}{\delta t} (\delta \tilde{\mathbf{u}}_h, \mathbf{v}_h) + (\tilde{\mathbf{u}}_h^{n+\theta} \cdot \nabla \tilde{\mathbf{u}}_h^{n+\theta}, \mathbf{v}_h) + (\nu \nabla \tilde{\mathbf{u}}_h^{n+\theta}, \nabla \mathbf{v}_h) \\ &= (p_h^n, \nabla \cdot \mathbf{v}_h) + (\mathbf{f}^{n+\theta}, \mathbf{v}_h) + (\boldsymbol{\sigma}^{n+\theta} \cdot \mathbf{n}, \mathbf{v}_h)_{\Gamma_{\text{nu}}}, \end{aligned} \quad (8)$$

$$\delta t (\nabla (p_h^{n+1} - p_h^n), \nabla q_h) = -(q, \nabla \cdot \tilde{\mathbf{u}}_h^{n+1}), \quad (9)$$

$$\frac{1}{\delta t} (\mathbf{u}_h^{n+1} - \tilde{\mathbf{u}}_h^{n+1}, \mathbf{v}_h) = (p_h^{n+1} - p_h^n, \nabla \cdot \mathbf{v}_h), \quad (10)$$

$\forall (\mathbf{v}_h, q_h) \in \mathbf{V}_h \times Q_h$. \mathbf{V}_h and Q_h are the standard finite element spaces where the velocity and the pressure is going to be approximated, \mathbf{v}_h and q_h their respective test functions. $\tilde{\mathbf{u}}_h$, \mathbf{u}_h and p_h are the intermediate velocity, the velocity and the pressure FE approximations, the subscript h refers to the discrete problem, and

$$(\mathbf{a}, \mathbf{b}) = \int_{\Omega} \mathbf{a} \cdot \mathbf{b} \, d\Omega, \quad (\mathbf{a}, \mathbf{b})_{\Gamma} = \int_{\Gamma} \mathbf{a} \cdot \mathbf{b} \, d\Gamma.$$

At this point, it is important to introduce the associated matrix structure of (8)-(10):

$$\begin{aligned} \mathbf{M} \frac{1}{\delta t} (\tilde{\mathbf{U}}^{n+1} - \mathbf{U}^n) + \mathbf{K} (\tilde{\mathbf{U}}^{n+\theta}) \tilde{\mathbf{U}}^{n+\theta} - \mathbf{G} \mathbf{P}^n \\ = \mathbf{F}^{n+\theta}, \end{aligned} \quad (11)$$

$$\delta t \mathbf{L} (\mathbf{P}^{n+1} - \mathbf{P}^n) = -\mathbf{D} \tilde{\mathbf{U}}^{n+1}, \quad (12)$$

$$\mathbf{M} \frac{1}{\delta t} (\mathbf{U}^{n+1} - \tilde{\mathbf{U}}^{n+1}) - \mathbf{G} (\mathbf{P}^{n+1} - \mathbf{P}^n) = \mathbf{0} \quad (13)$$

with \mathbf{M} is the standard mass matrix, \mathbf{K} the matrix from the advective and viscous contributions (the advective term has to be linearized, i.e. using a Picard or Newton-Raphson scheme), \mathbf{G} the matrix from the pressure gradient, \mathbf{F} the right hand side (RHS) terms, \mathbf{L} the standard laplacian matrix and \mathbf{D} the divergence matrix ($\mathbf{D} = \mathbf{G}^t$). $\tilde{\mathbf{U}}$, \mathbf{U} and \mathbf{P} are the vectors containing the $\tilde{\mathbf{u}}_h$, \mathbf{u}_h and p_h nodal values, respectively.

By having $\tilde{\mathbf{U}}^{n+1}$ from (13) and inserting the result in (11) and (12), the following system of equations is ob-

tained:

$$\begin{aligned} M \frac{1}{\delta t} (\mathbf{U}^{n+1} - \mathbf{U}^n) + \mathbf{K}(\mathbf{U}^{n+\theta}) \mathbf{U}^{n+\theta} - \mathbf{G} \mathbf{P}^n = \\ \mathbf{F}^{n+\theta} + \mathbf{E}(\mathbf{U}^{n+\theta}), \quad (14) \\ \mathbf{D} \mathbf{U}^{n+1} + \delta t (\mathbf{L} - \mathbf{D} \mathbf{M}^{-1} \mathbf{G}) (\mathbf{P}^{n+1} - \mathbf{P}^n) = \mathbf{0} \quad (15) \end{aligned}$$

The pressure stabilization effect of the method comes from the term $\delta t \mathbf{B} \mathbf{P}^{n+1}$, where $\mathbf{B} := \mathbf{L} - \mathbf{D} \mathbf{M}^{-1} \mathbf{G}$, which is a positive semi-definite matrix. Such result is formally demonstrated in [10]. The term $\mathbf{E}(\mathbf{U}^{n+\theta})$ in (14) is the error coming from the implicit treatment of the advective and viscous terms, which is (also formally demonstrated) of order $O(\delta t^2)$ (see equation (7)).

It is shown in [10] that the pressure stability of the above second order FS scheme holds only for δt large enough. In order to avoid the pressure instabilities for small δt , the formulation can be reinterpreted as a stabilized monolithic scheme following the cited reference.

3 Monolithic Stabilized Scheme

An analog monolithic stabilized formulation of problem (8)-(10), can be written as: Given \mathbf{u}_h^n , find $(\mathbf{u}_h^{n+1}, p_h^{n+1}, \boldsymbol{\xi}_h^{n+1})$ in $\mathbf{V}_h \times Q_h \times \tilde{\mathbf{V}}_h$ such that

$$\begin{aligned} \frac{1}{\delta t} (\delta \mathbf{u}_h, \mathbf{v}_h) + (\mathbf{u}_h^{n+\theta} \cdot \nabla \mathbf{u}_h^{n+\theta}, \mathbf{v}_h) + (\nu \nabla \mathbf{u}_h^{n+\theta}, \nabla \mathbf{v}_h) \\ - (p_h^{n+1}, \nabla \cdot \mathbf{v}_h) = (\mathbf{f}^{n+\theta}, \mathbf{v}_h) + (\boldsymbol{\sigma}^{n+\theta} \cdot \mathbf{n}, \mathbf{v}_h)_{\Gamma_{\text{nu}}}, \quad (16) \\ (q, \nabla \cdot \mathbf{u}_h^{n+1}) + \tau (\nabla p_h^{n+1} - \boldsymbol{\xi}_h^{n+1}, \nabla q_h) = 0, \quad (17) \\ (\boldsymbol{\xi}_h^{n+1}, \tilde{\mathbf{v}}_h) = (\nabla p_h^{n+1}, \tilde{\mathbf{v}}_h), \quad (18) \end{aligned}$$

$\forall (\mathbf{v}_h, q_h, \tilde{\mathbf{v}}_h) \in \mathbf{V}_h \times Q_h \times \tilde{\mathbf{V}}_h$ and $\delta \mathbf{u}_h = \mathbf{u}_h^{n+1} - \mathbf{u}_h^n$. The function space $\tilde{\mathbf{V}}_h$ is the same space \mathbf{V}_h but without boundary conditions. This is, (18) does not have any prescribed value. τ is the critical timestep to avoid spurious pressure oscillations, which turns out to be the same critical time step to integrate the advective term explicitly. The stability and convergence analysis dictates that it must behave as [2, 16, 9]:

$$\tau = \frac{h^2}{4\nu + 2|u|h} \quad (19)$$

where h and $|u|$ are the typical element size and element velocity. Therefore, this parameter has to be computed element by element in a real problem.

The matrix structure of (16)-(18) is:

$$M \frac{1}{\delta t} (\mathbf{U}^{n+1} - \mathbf{U}^n) + \mathbf{K}(\mathbf{U}^{n+\theta}) \mathbf{U}^{n+\theta}$$

$$- \mathbf{G} \mathbf{P}^{n+1} = \mathbf{F}^{n+\theta}, \quad (20)$$

$$\mathbf{D} \mathbf{U}^{n+1} + \tau (\mathbf{L} \mathbf{P}^{n+1} - \tilde{\mathbf{D}} \boldsymbol{\Xi}^{n+1}) = \mathbf{0}, \quad (21)$$

$$\tilde{\mathbf{M}} \boldsymbol{\Xi}^{n+1} = \tilde{\mathbf{G}} \mathbf{P}^{n+1} \quad (22)$$

where the matrices $\tilde{\mathbf{D}}$, $\tilde{\mathbf{M}}$ and $\tilde{\mathbf{G}}$ are the same \mathbf{D} , \mathbf{M} and \mathbf{G} matrices, but without boundary conditions. By putting $\boldsymbol{\Xi}^{n+1}$ in function of \mathbf{P}^{n+1} from (22), and inserting the result in (21), the following system of equations is obtained:

$$\begin{aligned} M \frac{1}{\delta t} (\mathbf{U}^{n+1} - \mathbf{U}^n) + \mathbf{K}(\mathbf{U}^{n+\theta}) \mathbf{U}^{n+\theta} \\ - \mathbf{G} \mathbf{P}^{n+1} = \mathbf{F}^{n+\theta}, \quad (23) \end{aligned}$$

$$\mathbf{D} \mathbf{U}^{n+1} + \tau (\mathbf{L} - \tilde{\mathbf{D}} \tilde{\mathbf{M}}^{-1} \tilde{\mathbf{G}}) \mathbf{P}^{n+1} = \mathbf{0} \quad (24)$$

which is very similar to the fractioned system (14)-(15). The main difference is that now, the stability problem is independent of δt , and that the error due to the implicit treatment of the advective and viscous terms ($\mathbf{E}(\mathbf{U}^{n+\theta})$ in (14)) is automatically eliminated.

At this point, it is important to find an efficient way to solve the stabilized monolithic formulation. The first idea was to solve (20)-(22) for each timestep in a staggered manner, using a block Gauss-Seidel or Jacobi type iteration. This is, for a given timestep, the non-symmetric system (20) is solved using a diagonal preconditioned GMRES (generalized method of residuals) algorithm, then, a CG-ILU (conjugate gradient preconditioned with an incomplete LU factorization) is used for the symmetric and positive semidefinite system (21), and finally, (22) is treated in an explicit manner by using a lumped approximation of \mathbf{M} . The algorithm is repeated until convergence into the timestep, and then, the variables are updated to go at the following time step.

However, in most of the cases, the whole system (20)-(22) is very ill-conditioned and the staggered solution does not converge at all. Then, the system must be preconditioned. To do that, the problem (20)-(22) can be fractioned again, obtaining the following FS stabilized scheme:

$$\begin{aligned} M \frac{1}{\delta t} (\tilde{\mathbf{U}}^{n+1} - \mathbf{U}^n) + \mathbf{K}(\tilde{\mathbf{U}}^{n+\theta}) \tilde{\mathbf{U}}^{n+\theta} \\ = \mathbf{G} \mathbf{P}^n + \mathbf{F}^{n+\theta}, \quad (25) \end{aligned}$$

$$\begin{aligned} \delta t \mathbf{L} (\mathbf{P}^{n+1} - \mathbf{P}^n) + \tau (\mathbf{L} \mathbf{P}^{n+1} - \tilde{\mathbf{D}} \boldsymbol{\Xi}^{n+1}) \\ = -\mathbf{D} \tilde{\mathbf{U}}^{n+1}, \quad (26) \end{aligned}$$

$$M \frac{1}{\delta t} (\mathbf{U}^{n+1} - \tilde{\mathbf{U}}^{n+1}) - \mathbf{G} (\mathbf{P}^{n+1} - \mathbf{P}^n) = \mathbf{0}, \quad (27)$$

$$\tilde{\mathbf{M}} \boldsymbol{\Xi}^{n+1} = \tilde{\mathbf{G}} \mathbf{P}^{n+1}. \quad (28)$$

This last FS scheme, adding the advective stabilizing terms that will be presented below, is very effective for

low Reynolds (Re) number problems [10]. Nevertheless, it was tested for a backward facing step problem at high Re number attaining convergence to the steady-state solution only for small δt , e.g. for δt of order 10^{-2} . The numerical experience pointed out that the source of the problem is the velocity correction step (27) (note that the correction is multiplied by δt). It is clear that for the steady-state solution such step can be omitted. Doing this for the mentioned high Re number problem, the convergence was attained for all timestep sizes. Finally, note that for the monolithic formulation the velocity correction step does not appear, therefore, the problem was reformulated as follows.

First, \tilde{U}^{n+1} was obtained from (27) and the result was inserted in (25) to arrive at the following system:

$$M \frac{1}{\delta t} (\mathbf{U}^{n+1} - \mathbf{U}^n) + \mathbf{K} (\mathbf{U}^{n+\theta}) \mathbf{U}^{n+\theta} - \mathbf{G} \mathbf{P}^n = \mathbf{F}^{n+\theta} + \mathbf{E} (\mathbf{U}^{n+\theta}), \quad (29)$$

$$\delta t \mathbf{L} (\mathbf{P}^{n+1} - \mathbf{P}^n) + \tau (\mathbf{L} \mathbf{P}^{n+1} - \tilde{\mathbf{D}} \boldsymbol{\Xi}^{n+1}) = -\mathbf{D} \tilde{\mathbf{U}}^{n+1}, \quad (30)$$

$$M \frac{1}{\delta t} (\mathbf{U}^{n+1} - \tilde{\mathbf{U}}^{n+1}) - \mathbf{G} (\mathbf{P}^{n+1} - \mathbf{P}^n) = \mathbf{0}, \quad (31)$$

$$\tilde{\mathbf{M}} \boldsymbol{\Xi}^{n+1} = \tilde{\mathbf{G}} \mathbf{P}^{n+1} \quad (32)$$

where $\mathbf{E} (\mathbf{U}^{n+\theta})$ is the FS implicit error of $O(\delta t^2)$ (see (7)). However, such term can be eliminated as in (20)-(22) by writing the following analog monolithic scheme:

$$M \frac{1}{\delta t} (\mathbf{U}^{n+1} - \mathbf{U}^n) + \mathbf{K} (\mathbf{U}^{n+\theta}) \mathbf{U}^{n+\theta} - \mathbf{G} \mathbf{P}^{n+1} = \mathbf{F}^{n+\theta}, \quad (33)$$

$$\delta t \mathbf{L} (\mathbf{P}^{n+1} - \mathbf{P}^n) + \tau (\mathbf{L} \mathbf{P}^{n+1} - \tilde{\mathbf{D}} \boldsymbol{\Xi}^{n+1}) = -\mathbf{D} \mathbf{U}^{n+1}, \quad (34)$$

$$\tilde{\mathbf{M}} \boldsymbol{\Xi}^{n+1} = \tilde{\mathbf{G}} \mathbf{P}^{n+1} \quad (35)$$

It is easy to see that the problem (33)-(35) is exactly the same than the stabilized monolithic problem (20)-(22), except for the term $\delta t \mathbf{L} (\mathbf{P}^{n+1} - \mathbf{P}^n)$ in (34). This is a positive definite (\mathbf{L} is the standard Laplacian matrix) $O(\delta t^2)$ term, which preconditions the whole system (20)-(22), and allows the staggered Gauss-Seidel type uncoupled solution proposed before to converge.

It is clear that the steady-state solution of (33)-(35) is exactly the same than the solution of the stabilized monolithic problem (20)-(22). However, the transient results could be slightly different (only order $O(\delta t^2)$ different) due to the preconditioning second order term. Such small shortcoming can be easily removed but rewriting such term as $\delta t \mathbf{L} (\mathbf{P}^{n+1,i} - \mathbf{P}^{n+1,i-1})$, where the superscript i

refers to the number of the block Gauss-Seidel iteration into the time step. Then, the final uncoupled monolithic scheme using a Picard linearization for the advective term can be written as follows:

$$M \frac{1}{\delta t} (\mathbf{U}^{n+1,i} - \mathbf{U}^n) + \mathbf{K} (\mathbf{U}^{n+\theta,i-1}) \mathbf{U}^{n+\theta,i} - \mathbf{G} \mathbf{P}^{n+1,i-1} = \mathbf{F}^{n+\theta}, \quad (36)$$

$$\delta t \mathbf{L} (\mathbf{P}^{n+1,i} - \mathbf{P}^{n+1,i-1}) + \tau (\mathbf{L} \mathbf{P}^{n+1,i} - \tilde{\mathbf{D}} \boldsymbol{\Xi}^{n+1,i-1}) = -\mathbf{D} \mathbf{U}^{n+1,i}, \quad (37)$$

$$\tilde{\mathbf{M}}_l \boldsymbol{\Xi}^{n+1,i} = \tilde{\mathbf{G}} \mathbf{P}^{n+1,i} \quad (38)$$

where $\tilde{\mathbf{M}}_l$ is the lumped mass matrix. Basically, in this final formulation the convergence of the block Gauss-Seidel uncoupled solution is enforced by the first term of (37), while the pressure stability is attained by the second term of the same equation.

4 Pressure Stabilizing Term

If the second term of (37), which comes from the bilinear form $(\tau(\nabla p_h - \xi_h), \nabla q_h)$, is computed in the center of the edge (element) $(k, k+1)$ of a one dimensional problem using linear elements of size h , the following contribution is obtained at the left hand side (LHS) of (37):

$$\tau \left(\frac{p_{k+1} - p_k}{h} - \frac{p_{k+1} - p_{k-1}}{4h} - \frac{p_{k+2} - p_k}{4h} \right) \quad (39)$$

which can be re-written at the right hand side as:

$$-\frac{\tau}{h} \left(p_k - p_{k+1} + \frac{h}{2} (\nabla p_k + \nabla p_{k+1}) \right) \quad (40)$$

where ∇p_k is the second order finite difference gradient of p evaluated at nodal point k , this is $\nabla p_k = (p_{k+1} - p_{k-1})/2h$. The (40) term is exactly the same higher order term presented by Löhner et al. in [20, 21], and is equivalent to a fourth-order damping term for the divergence equation. In such reference, the term added to the mesh edge (i, j) at the RHS of the equation is:

$$-\frac{\delta t}{l_{ij}} \left(p_i - p_j + \frac{l_{ij}}{2} (\nabla p_i + \nabla p_j) \right) \quad (41)$$

where δt is the critical time step to integrate explicitly the advective term, and l_{ij} the edge length. Taking into account that τ is the critical time step, (40) and (41) are exactly the same pressure stabilizing expressions.

As a final remark, if the contributions of the two edges surrounding the nodal point k are written down, it can be seen that the final LHS stencil for the equation k is:

$$\mathcal{S}_k = \frac{\tau}{h} \left(\frac{1}{4} p_{k-2} - p_{k-1} + \frac{3}{2} p_k - p_{k+1} + \frac{1}{4} p_{k+2} \right) \quad (42)$$

If the Taylor expansions for p_{k-2} , p_{k-1} , p_{k+1} and p_{k+2} around p_k are introduced in (42), one obtains:

$$\mathcal{S}_k = \frac{\tau}{h} \frac{3}{12} h^4 \frac{d^4 p_k}{dx^4} + O(h^6). \quad (43)$$

Then, taking into account that τ is proportional to h or to h^2 for convective or viscous dominated flows respectively (see (19)), the pressure stabilizing term is formally at least a fourth order term.

5 Advective Stabilization

In this work, the advective term of the NS equations was stabilized by using a high order SUPG (Streamline Upwind Petrov Galerkin) formulation, based on the higher order stabilization used for the pressure. Basically, the final discrete problem is as follows: Given \mathbf{u}_h^n , find $(\mathbf{u}_h^{n+1}, p_h^{n+1}, \boldsymbol{\pi}_h^{n+1}, \boldsymbol{\xi}_h^{n+1})$ in $\mathbf{V}_h \times Q_h \times \tilde{\mathbf{V}}_h \times \tilde{\mathbf{V}}_h$ such that

$$\begin{aligned} & \frac{1}{\delta t} (\mathbf{u}_h^{n+1,i} - \mathbf{u}_h^n, \mathbf{v}_h) + (\mathbf{u}_h^{n+\theta,i-1} \cdot \nabla \mathbf{u}_h^{n+\theta,i}, \mathbf{v}_h) \\ & + (\nu \nabla \mathbf{u}_h^{n+\theta,i}, \nabla \mathbf{v}_h) - (p_h^{n+1,i-1}, \nabla \cdot \mathbf{v}_h) + \\ & (\tau (\mathbf{u}_h^{n+\theta,i-1} \cdot \nabla \mathbf{u}_h^{n+\theta,i} - \boldsymbol{\pi}_h^{n+\theta,i-1}), \mathbf{u}_h^{n+\theta,i-1} \cdot \nabla \mathbf{v}_h) \\ & = (\mathbf{f}^{n+\theta}, \mathbf{v}_h) + (\boldsymbol{\sigma}^{n+\theta,i-1} \cdot \mathbf{n}, \mathbf{v}_h)_{\Gamma_{\text{nu}}}, \quad (44) \\ & \delta t (\nabla p_h^{n+1,i} - \nabla p_h^{n+1,i-1}, \nabla q_h) + \\ & (\tau (\nabla p_h^{n+1,i} - \boldsymbol{\xi}^{n+1,i-1}), \nabla q_h) = -(\nabla \cdot \mathbf{u}_h^{n+1,i}, q_h), \quad (45) \\ & (\boldsymbol{\pi}_h^{n+\theta,i}, \tilde{\mathbf{v}}_h) = (\mathbf{u}_h^{n+\theta,i} \cdot \nabla \mathbf{u}_h^{n+\theta,i}, \tilde{\mathbf{v}}_h), \quad (46) \\ & (\boldsymbol{\xi}_h^{n+1,i}, \tilde{\mathbf{v}}_h) = (\nabla p_h^{n+1,i}, \tilde{\mathbf{v}}_h), \quad (47) \end{aligned}$$

$\forall (\mathbf{v}_h, q_h, \tilde{\mathbf{v}}_h, \tilde{\mathbf{v}}_h) \in \mathbf{V}_h \times Q_h \times \tilde{\mathbf{V}}_h \times \tilde{\mathbf{V}}_h$. The superscript i stands for the block Gauss-Seidel iteration number into the timestep, and the critical timestep τ has been introduced into the discrete forms to indicate that it has to be computed element by element.

In the above formulation, the advective term are stabilized by the fifth LHS term of (44), which is the subtraction of the classical streamline diffusion term [4, 25] and its projection onto the finite element space. In this sense, the stabilizing term is the orthogonal projection of the classical SUPG term onto the finite element space. Furthermore, observe that if the advective operator $\mathbf{u} \cdot \nabla(\cdot)$ is replaced by the pressure one $\nabla(\cdot)$ in the residual and the test function terms, the advective and pressure stabilization terms are exactly the same. Then, the one dimensional stencil of the advective stabilization term is equal as the stencil presented in equation (39), replacing p by \mathbf{u} and τ by $\tau|\mathbf{u}|^2$, which makes it a high order streamline diffusion.

The stabilization methods presented in this work has been generalized by Codina in [11, 12] as the OSS (orthogonal sub-scales stabilization) method. The main difference with the method presented in this work, is the preconditioning term $\delta t (\nabla p_h^{n+1,i} - \nabla p_h^{n+1,i-1}, \nabla q_h)$ used to enforce the convergence of the block Gauss-Seidel uncoupled solution, of the final monolithic system of equations.

Finally, the 1D stencil for the node k of the convective terms, Galerkin and stabilized contributions (2nd and 5th LHS terms of (44)), in a uniform mesh of size h is:

$$\mathcal{L}_k = \frac{1}{8} a (u_{k-2} - 8u_{k-1} + 6u_k + u_{k+2}) \quad (48)$$

where $a = u_h^{n+\theta,i-1}$ is the advective velocity, and $u_j = u_{h_j}^{n+\theta,i}$ the unknown. Then, using Taylor expansions around u_k , it can be demonstrated that such terms is a formal second order discretization of the convective operator with the form:

$$a \frac{du_k}{dx} = \frac{1}{h} \mathcal{L}_k - \frac{h^2}{6} \frac{d^3 u_k}{dx^3} + O(h^3) \quad (49)$$

REMARK 1: Note that the method is consistent. The solution of (1)-(2) is solution of (44)-(47), and when the mesh size h tends to zero, not only the stabilizing ‘‘viscosity’’ τ (see equation (19)) tends to zero, but also the stabilizing pressure and advective residual terms $(\nabla p_h^{n+1,i} - \boldsymbol{\xi}^{n+1,i-1}$ and $\mathbf{u}_h^{n+\theta,i-1} \cdot \nabla \mathbf{u}_h^{n+\theta,i} - \boldsymbol{\pi}_h^{n+\theta,i-1})$. In addition, if $\theta = 0.5$ is used for the trapezoidal rule (Crank Nicholson), it is formally second order accurate in time, and it is clear from the discrete form (44)-(47), that the steady-state solution does not depend on the timestep size.

6 Monotonicity Preserving Term

The high order streamline diffusion could not avoid localized oscillations, overshoot and undershoots, which may deteriorate the convergence of the formulation. Even though most of the numerical problems that have been solved to date have not presented such anomalies, a type of non-linear numerical switch had to be designed for some of them to avoid local spurious oscillations.

The idea is to identify the strongly convective flow regions by the difference between the convective term and its projection. Then, at each iteration, a variable β is computed within each element as:

$$\beta = \frac{\|\mathbf{u}_h \cdot \nabla \mathbf{u}_h - \boldsymbol{\pi}_h\|}{\|\mathbf{u}_h \cdot \nabla \mathbf{u}_h\| + \|\boldsymbol{\pi}_h\|} \quad (50)$$

where $\|\cdot\|$ is the euclidian norm of the vector enclosed. It is straightforward to see that $0 \leq \beta \leq 1$, taking values close to zero where the velocity field presents a smooth variation, and close to one in flow regions having sharp gradients.

Hence, a numerical switch to lower the discretization order in such sharp gradient regions, is obtained by multiplying the high order SUPG term (last LHS term in (44)) by:

$$\alpha = \min\{1, C(1 - \beta)\} \quad (51)$$

with $C \geq 1$ constant. In general $C = 2$, which means that for values of β between zero and 0.5 (smooth zones) the convective term discretization is formally second order, and for higher values of β (sharp gradient regions) it goes from second to first order, obtaining over/undershoot free solutions. As mentioned before, for most of the numerical problems α was taken to 1 (formally second order SUPG discretization). This was the case of all the numerical examples presented in this work.

7 Numerical Examples

7.1 Backward-Facing Step

The first example considered is the laminar backward-facing step at different Re numbers. It was performed to verify the effectivity of the monolithic formulation (44)-(47) and of the block Gauss-Seidel uncoupled solution scheme, to deal with steady-state problems at low and high Re . The problem geometry and mesh is shown in Figure 1 (the vertical direction has been scaled in all the plots). Aspect ratio of the backward-facing step H to the overall sectional width is 1:2 and the total length in the horizontal direction is $20H$. A fully developed parabolic velocity profile is prescribed at the inflow boundary. At the outflow, the pressure and the viscous stresses were set to zero. The mesh is composed of 990 linear triangles and 544 nodal points.

According Armaly et al. [1], the Re number will be based on the average value of the inlet velocity profile and the cross-sectional width of the whole domain. For $Re < 500$, there exists only one recirculation zone behind the step. For higher values of Re , another recirculation zone appears at the top wall of the channel. Experimental results indicate that a third recirculation zone appears at the bottom of the wall for values of $Re > 1000$.

The numerical results agree very well for $Re < 600$ with those that can be found in the above mentioned reference. For brevity, they have not been included here, and

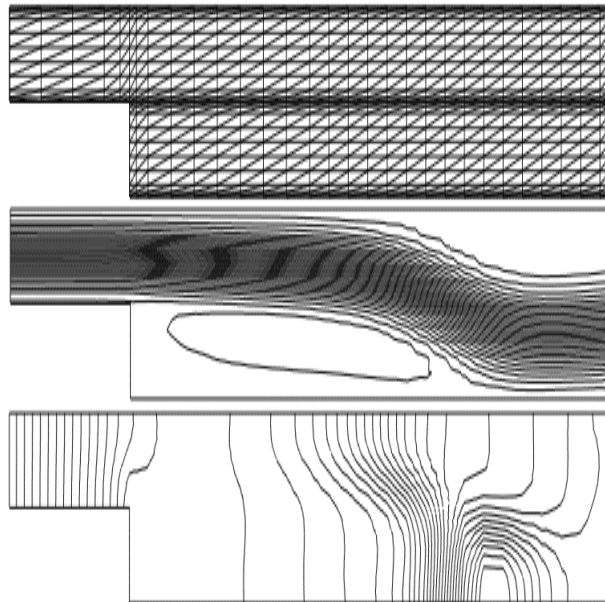


Figure 1: From top to bottom: Mesh of 990 linear elements and 544 nodal points. Streamline pattern. Pressure contours; peaks $(-0.6208, 0.1979)$.

only those for $Re = 1000$ are included. For such high Re number, the stabilized second order FS scheme (25)-(28), failed to converge for large δt (it only converged for timestep size of order 10^{-2}) as was mentioned before. However, the final monolithic scheme (44)-(47) was very effective, it converged to the same steady-state solution for δt from 0.01 to 1.0. In addition, the convergence was held not only by using the backward Euler scheme $\theta = 1.0$, but also using the Crank Nicholson scheme $\theta = 0.5$, which, as it is well known, is less dissipative. In Figure 1 the streamline pattern is presented. The length of the vortex behind the step is approximately 13.0, and the experimental result is 14.3. Taking into account that some discrepancies should be expected due to the three-dimensionality of the experimental flow at this Re number, the results is good. Due to the length of the channel, the other two recirculation zones could not be captured completely. However, the important result is the excellent convergence of the numerical scheme for high Re numbers. Finally, in Figure 1 the pressure field is presented. Note that there are no pressure reflections at the outflow. The pressure gradient is parallel to the horizontal direction.

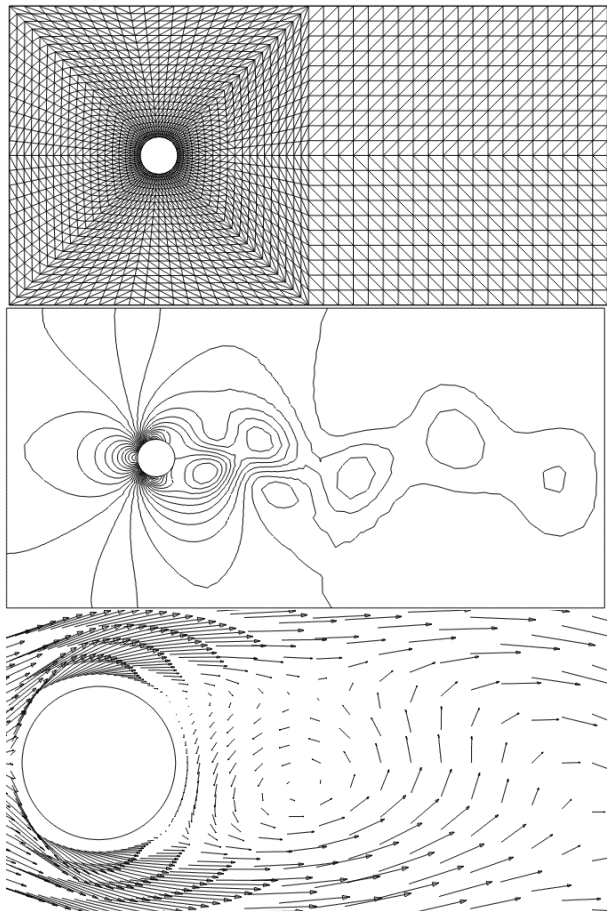


Figure 2: From top to bottom: Mesh of 4.000 linear elements and 2.100 nodal points. Pressure contours at $t = 35.5$; peaks $(-0.7657, 0.6855)$.

7.2 Vortex Shedding Behind a Cylinder

This example involves the flow past a cylinder, another widely solved benchmark problem. A circular cylinder is immersed in a viscous fluid. The Re number is based on the diameter and the prescribed inflow velocity. The mesh and geometry are shown in Figure 2. The flow domain is the rectangle $[0, 0] \times [16, 8]$ minus the circle of diameter 1.0 and center coordinates $[4, 4]$. For $Re < 40$, two symmetric eddies develop behind the cylinder. These eddies become unstable at higher Re , and periodic vortex occurs leading to the so called von Karman vortex street. The case $Re = 100$ is usually considered as the standard test to check the time accuracy of incompressible flow numerical schemes. The period of the oscillations for such Re number found in the literature is around 6.0 approximately [4, 17, 15].

In this work two cases were tested. The $Re = 100$

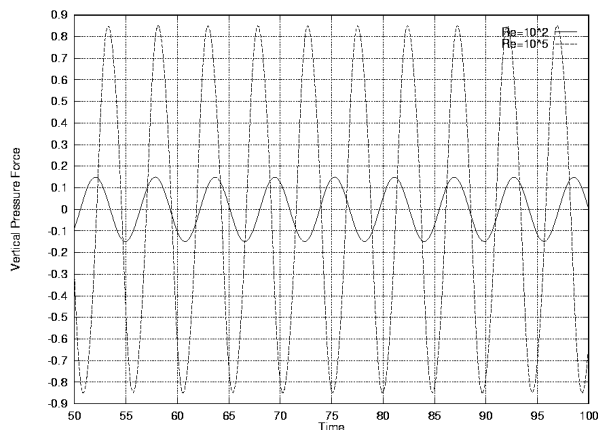


Figure 3: Time evolution of the vertical pressure force over the cylinder.

standard one, and a turbulent case at $Re = 10^5$. For the laminar case, no-slip conditions were prescribed on the cylinder surface $\mathbf{u} = (0, 0)$. For the turbulent one, $(\mathbf{n} \cdot \boldsymbol{\sigma}) \cdot \hat{\mathbf{u}} = \tau_{wall}$ and $\mathbf{u} \cdot \mathbf{n} = 0$ was prescribed on the cylinder, where \mathbf{n} is the unit exterior normal vector, and $\hat{\mathbf{u}}$ is the unit vector in the velocity direction (which is tangent to the wall). $\tau_{wall} = -C_w |\mathbf{u}|^2$ and C_w is a positive constant which was set to 0.03 for the example. For both cases, the laminar and the turbulent one, the velocity was prescribed to $\mathbf{u} = (1, 0)$ at inflow, and at the top and bottom boundaries. At outflow, the pressure and the viscous stresses were set to zero. The turbulent model used for the $Re = 10^5$ case was Smagorinsky, which adds a elemental turbulent viscosity of:

$$\nu_t = C h^2 \sqrt{2\varepsilon(\mathbf{u}) : \varepsilon(\mathbf{u})} \quad (52)$$

where $C = 0.01$ is a positive constant, h the element size, $\varepsilon(\mathbf{u})$ the velocity symmetric-gradient tensor, and $(\cdot) : (\cdot)$ the tensorial scalar product.

Figure 2 presents the pressure field and a detail of the velocities around the cylinder for a given time step. The main results are shown in Figure 3, where the vertical pressure force over the cylinder is plotted for both cases. The period for $Re = 100$ laminar case is approximately 6.1 which is in good agreement with the reported ones. For $Re = 10^5$, it is around 4.8, but the wave amplitude is higher. Such values strongly depend on the chosen value for C_w . For both cases $\theta = 0.5$ (Crank Nicholson scheme, second order accurate) was used for the temporal discretization, and a timestep size of 0.1 which corresponds to a Courant number of 4.0 approximately. If θ is set to $\theta = 1.0$ (backward Euler scheme, first order accurate), the wave amplitude decreased a 50% approximately, but

the period is maintained. This is the typical behaviour of the first order Backward Euler scheme, which present errors in the wave amplitude but not in its phase.

7.3 Model of a Carotid Stenosis

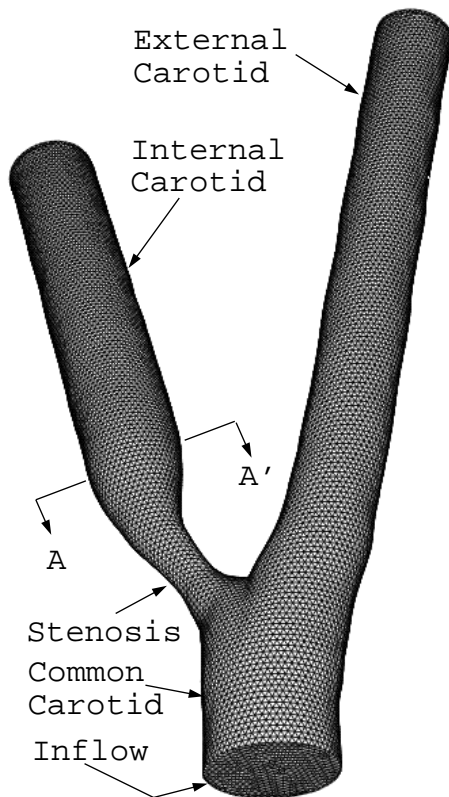


Figure 4: Surface mesh and cut position. Volume mesh of 416.939 tetrahedrals and 78.822 nodes.

This first 3D example consist of computing the blood flow in a glass prototype of the carotid arteries, with a 65% of diameter reduction (stenosis) at the internal carotid (ICA) junction. In Figure 4 the surface mesh, and the cut position (A-A') where experimental results are available, are shown. Such empirical data were obtained by phase-contrast MRA (Magnetic Resonance Angiography, see [5] for details). The Reynolds number of the problem based on the maximum velocity ($u = 40\text{cm/seg}$) and diameter ($\phi = 0.8\text{cm}$) at inflow, is approximately 740. The boundary conditions are: Velocity equal zero at solid walls, constant parabolic velocity profile at inflow and at the external carotid outflow (the flow in such branch was set to 57% of the injected one based on the experimental measurements), and $p = 0$ at the ICA outflow.

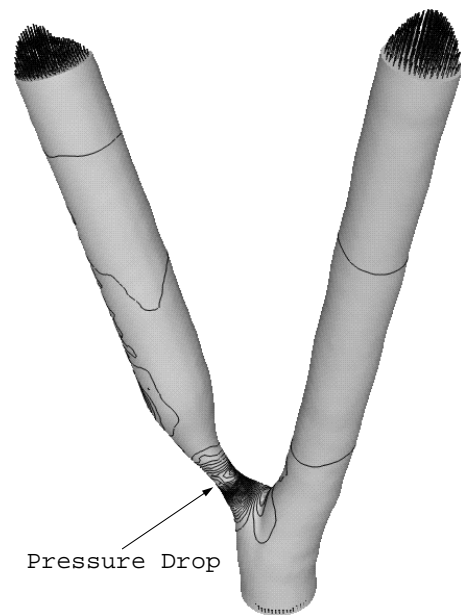


Figure 5: Pressure distribution and velocities at boundary.

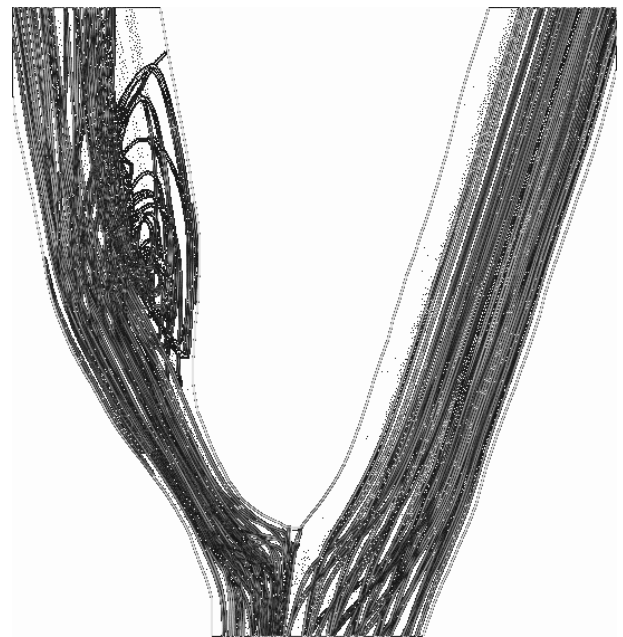


Figure 6: Recirculation zone produced by the Stenosis.

In Figure 5 the steady state pressure field and boundary velocity vectors are presented. The high pressure drop around the stenosis is well captured. In Figure 6 the strong recirculation zone produced by the contraction can also be observed. Finally, in Figure 7, a comparison between the computed and experimental velocity fields is presented. A very good agreement in the velocity pattern was obtained. Moreover, the velocity peaks were also captured: The error between the experimental and numerical values falls into the error margin of the measurements.

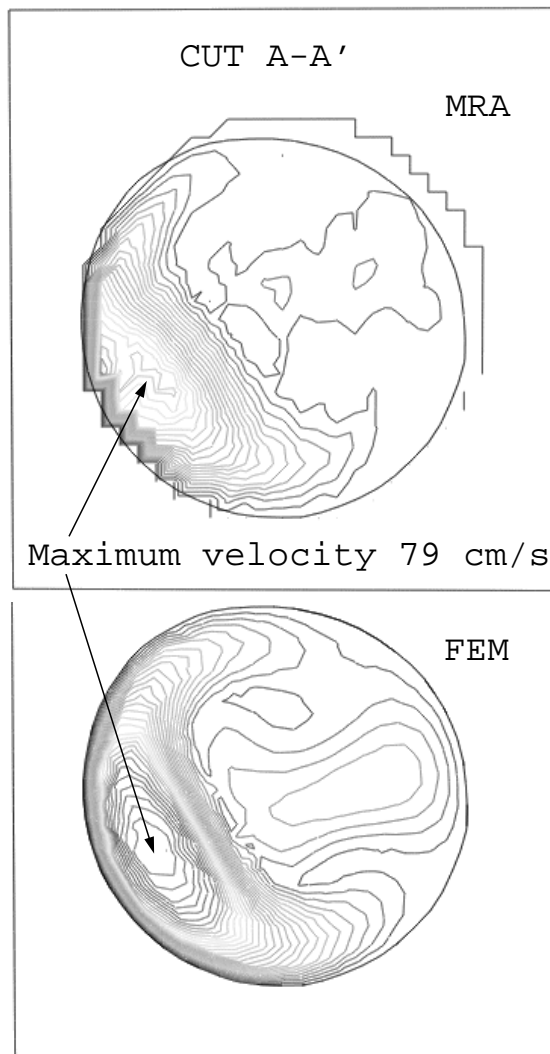


Figure 7: From top to bottom: Experimental velocity contours obtained by MRA. Numerical velocity contours obtained by FEM (Finite Element Method).

7.4 Blood Flow in the Circle of Willis

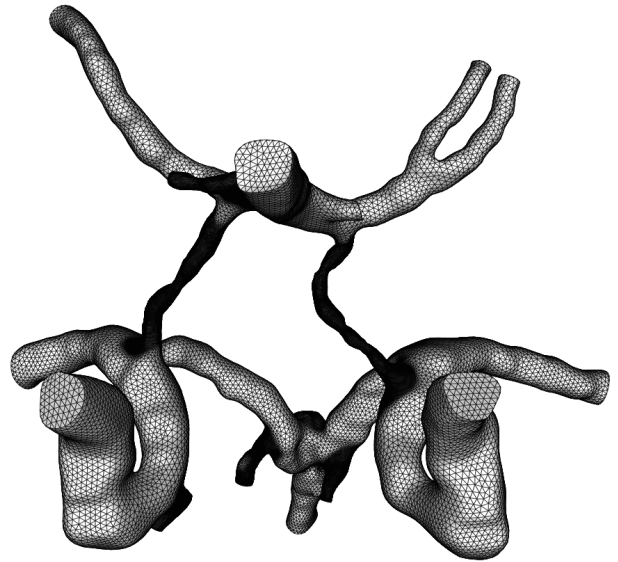


Figure 8: Surface mesh. Volume mesh of 3,997,447 linear elements and 726,270 nodal points.

This transient example is a real 3D case, which is included here to evaluate the computer time savings using the implicit monolithic scheme, compared with a second order accurate explicit FS method. The problem consist of computing the blood flow rate at the outlets of a portion of the brain arteries (Circle of Willis), by imposing a periodic inlet flow rate curve. In Figure 8 the surface mesh of the problem is presented. The volume mesh consisted of 3,997,447 linear elements and 726,270 nodal points. In Figure 9, the flow pattern for a specific time step is presented before and after one of the arteries was temporarily clipped, and also the shear stress field. The temporary clipping is a common neuro-surgical procedure to facilitate aneurysm elimination.

This problem was run using a timestep size of 0.012, which corresponds to 64 time steps for flow rate period. The critical time step that had to be used for the explicit solver was of the order of 10^{-5} , which is three orders of magnitude smaller than the timestep used for the implicit scheme. Even though the explicit solver time solution is cheaper than the implicit one, the implicit scheme was more than 10 times faster than the explicit method to simulate three periods of the flow.

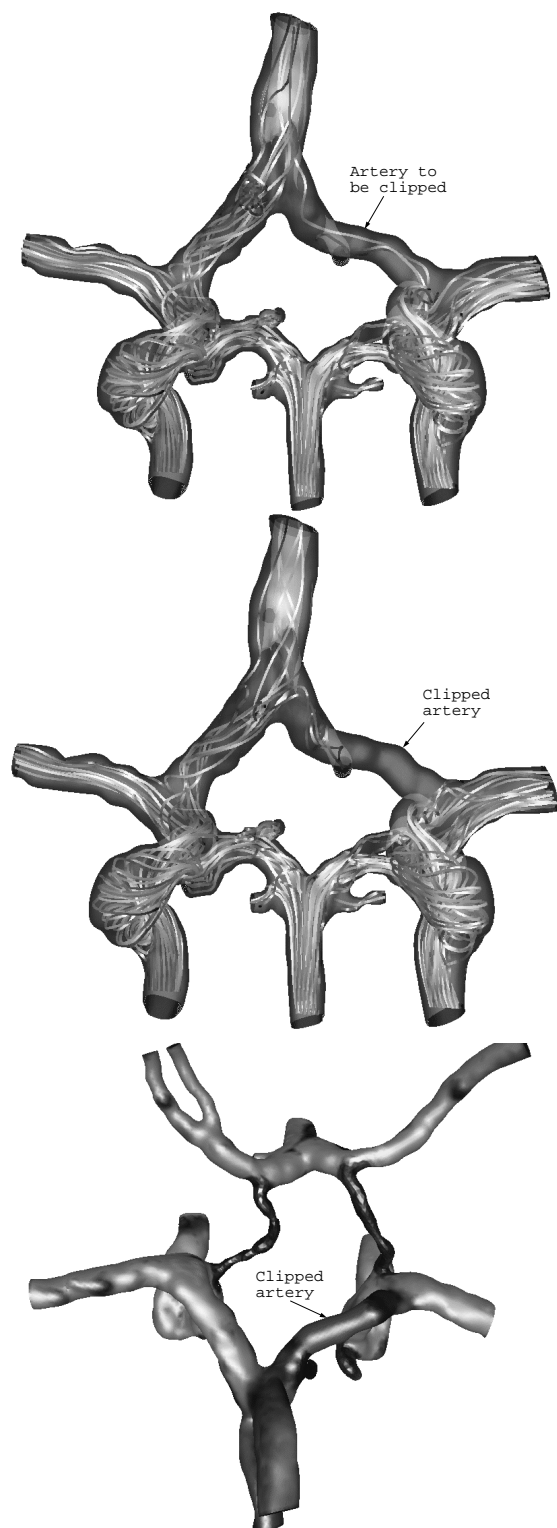


Figure 9: From top to bottom: Streamlines before and after clipping, and shear stress after clipping.

8 Conclusions

An implicit second-order accurate monolithic scheme was presented to solve incompressible flow problems. The final system of equations resulting from the time and space discretization are solved in each time step in an uncoupled manner, by using a block Gauss-Seidel type algorithm, and a preconditioner for the pressure (or incompressibility) equation.

The incompressible and convective terms were stabilized using an OSS scheme. For the incompressibility equation, it was demonstrated that such methods reduce to the same fourth order pressure term added by some authors to obtain high order accurate results. For the convective one, it was shown that the OSS stabilization is nothing but a second order approximation of the respective convective operator. The numerical experience indicates that the formulation is very efficient for all Reynolds numbers, and that its time accuracy is excellent. Such scheme seems to be very efficient for transient cases, when the critical time step of the problem is some orders of magnitude smaller than the time step requires to obtain time-accurate results (physical timestep). Furthermore, a numerical switch was developed to avoid spurious under and overshoots that may appear in high gradient zones.

Finally, four numerical examples (two bidimensional and two real 3D cases) were presented, which demonstrated the performance of the proposed methodology.

9 Acknowledgments

This work was partially funded by NRL LCP&FD. Dr. William Sandberg was the technical monitor.

References

- [1] B. Armaly, F. Durst, J. Pereira, and B. Schoning. Experimental and theoretical investigation of backward-facing step flow. *J. Fluid Mech.*, 127:473–476, 1983.
- [2] M. Behr and T. Tezduyar. Finite element solution strategies for large-scale flow simulations. *Comp. Meth. Appl. Mech. Eng.*, 112:3–24, 1994.
- [3] J. Bell, P. Colella, and H. Glaz. A second order projection method for the Navier-Stokes equations. *J. Comp. Phys.*, 85:257–283, 1989.
- [4] A. Brooks and T. Hughes. Streamline upwind/Petrov-Galerkin formulations for convection dominated flows with particular emphasis

- on the incompressible Navier-Stokes equation. *Comp. Meth. Appl. Mech. Eng.*, 32:199–259, 1982.
- [5] J. Cebal, P. Yim, R. Löhner, O. Soto, H. Marcos, and P. Choyke. New methods for computational fluid dynamics of carotid artery from magnetic resonance angiography. *Proc. SPIE Medical Imaging, Vol. 4321, paper No. 22, San Diego, California - February*, 2001.
- [6] Y. H. Choi and C. L. Merkle. The application of preconditioning in viscous flows. *J. Comp. Phys.*, 105:207–233, 1993.
- [7] A. Chorin. A numerical method for solving incompressible viscous problems. *J. Comp. Phys.*, 2:12–26, 1967.
- [8] A. Chorin. On the convergence of discrete approximation to the Navier-Stokes equations. *Math. Comput.*, 23, 1969.
- [9] R. Codina. A stabilized finite element method for generalized stationary incompressible flows. *Comp. Meth. Appl. Mech. Eng.*, Accepted for publication, 1999.
- [10] R. Codina. Pressure stability in fractional step finite element methods for incompressible flows. *J. Comp. Phys.*, Submitted for publication, 2000.
- [11] R. Codina. Stabilization of incompressibility and convection through orthogonal sub-scales in finite element methods. *Comp. Meth. Appl. Mech. Eng.*, Accepted for publication, 2000.
- [12] R. Codina. Stabilized finite element approximation of the Oseen equations using orthogonal subscales. *SIAM J. Numer. Anal.*, Submitted for publication, 2000.
- [13] R. Codina and O. Soto. Finite element solution of the Stokes problem with dominating Coriolis force. *Comp. Meth. Appl. Mech. Eng.*, 142:215–234, 1997.
- [14] G. Cowles and L. Martinelli. Fully non-linear hydrodynamic calculations for ship design on parallel computing platforms. In *Proc. 21st Symp. on Naval Hydrodynamics, Trondheim, Norway*, 1996.
- [15] M. Engelman and M. Jamnia. Transient flow past a circular cylinder: A benchmark solution. *Int. J. Numer. Meth. Fluids*, 11:985–1000, 1990.
- [16] L. Franca and S. Frey. Stabilized finite element methods: II. The incompressible Navier-Stokes equations. *Comp. Meth. Appl. Mech. Eng.*, 99:209–133, 1992.
- [17] P. Gresho, S. Chan, R. Lee, and C. Upson. A modified finite element method for solving the time-dependent, incompressible Navier-Stokes equations. *Int. Jour. Num. Meth. Fluids.*, 4:619–640, 1984.
- [18] T. Hino. A unstructured grid method for incompressible viscous flows with a free surface. *AIAA-97-0862*, 1997.
- [19] J. Kim and P. Moin. Application of a fractional-step method to incompressible Navier-Stokes equations. *J. Comp. Phys.*, 59:308–323, 1985.
- [20] R. Löhner, C. Yang, E. Oñate, and S. Idelsohn. An unstructured grid-based, parallel free surface solver. *AIAA-97-1830*, 1997.
- [21] R. Löhner, C. Yang, E. Oñate, and S. Idelsohn. An unstructured grid-based, parallel free surface solver. *Applied Numerical Mathematics*, 31:271–293, 1999.
- [22] D. Martin and R. Löhner. An implicit linelet-based solver for incompressible flows. *AIAA-92-0668*, 1992.
- [23] L. Martinelli and J. R. Farmer. *Sailing through the nineties: Computational fluid dynamics for ship performance analysis and design*. Chapter 27 in *Frontiers of Computational Fluid Dynamics* (D.A. Caughey and M.M. Hafez eds.), J. Wiley, 1994.
- [24] J. Peraire, K. Morgan, and J. Peiro. *The simulation of 3D incompressible flows using unstructured grids*. Chapter 16 in *Frontiers of Computational Fluid Dynamics* (D.A. Caughey and M.M. Hafez eds.), J. Wiley, 1994.
- [25] R. Ramamurti and R. Löhner. A parallel implicit incompressible flow solver using unstructured meshes. *Computer and Fluids*, 5:119–132, 1996.
- [26] A. Rizzi and L. Eriksson. Computation of inviscid incompressible flow with rotation. *J. Fluid Mech.*, 153:275–312, 1985.
- [27] T. Turkel. Preconditioned methods for solving the incompressible and low speed compressible equations. *J. Comp. Phys.*, 72:277–298, 1987.
- [28] J. M. Weiss and W. A. Smith. Preconditioning applied to variable and constant density time-accurate flows on unstructured grids. *AIAA J.*, 33, 1995.